Pergamon

0022-4073(95)00129-8

J. Quant. Spectrosc. Radiat. Transfer Vol. 54, No. 6, pp. 931–943, 1995

0022-4073/95 $9.50 + 0.00

EVIDENCE OF THE ZEEMAN SPLITTING IN THE $2_1 \rightarrow 0_1$ ROTATIONAL TRANSITION OF THE ATMOSPHERIC $^{16}O^{18}O$ MOLECULE FROM GROUND-BASED MEASUREMENTS

J. R. PARDO,†‡§ L. PAGANI,† M. GERIN,†‖ and C. PRIGENT†

†DEMIRM, URA336 du CNRS, Observatoire de Paris-Meudon, 61 Avenue de l'Observatoire, 75014 Paris, France, ‡Centro Astronómico de Yebes (OAN,IGN), Apartado 148, 19080 Guadalajara, Spain, and ‖Radioastronomie Millimétrique, URA336 du CNRS, ENS, 24 Rue Lhomond, 75005 Paris, France

(Received 2 March 1995)

Abstract—We present in this paper a set of spectra of the atmospheric $^{16}O^{18}O$ molecule taken at 233.94611 GHz with the 2.5 m-radiotelescope POM-2 located at Plateau de Bure (Lat. 44:38:02.00 N, Long. 5:54:28.50 E, Alt. 2550 m) in the French Alps. These spectra clearly show a Zeeman substructure over a ± 2.5 MHz range from the line centre. The central frequencies for each peak would indicate local mean values of the geomagnetic field over Plateau de Bure for the altitude range 2.5–130 km of around 40 μT that is a slight, but measurable, difference with respect to a standard geomagnetic model based on measurements carried out in 1980, that gives values around 44 μT. Depending on the direction and polarization we see 2, 4, or 6 peaks that are identified as π ($\Delta M = 0$) or $\sigma \pm$ ($\Delta M = \pm 1$) components. This effect cannot be seen from ground-based measurements in the millimetric lines of the main isotope $^{16}O_2$ for which very broad emission and high opacity of low layers eliminate any structure, but it must be taken into account for atmospheric temperature soundings from satellite at frequencies close to these $^{16}O_2$ resonances.

1. INTRODUCTION

The O_2 molecule in its ground electronic state has a permanent magnetic dipole moment coming from two parallel electron spins. In this state each rotational level, with quantum number N is split into 3 levels of total quantum number J (N_J) following a Hund's (b) coupling case. Since the nuclear spin is 0 the Bose–Einstein rule for symmetry of the total wavefunction imposes N to be odd in the case of $^{16}O_2$. However, N can also be even for $^{16}O^{18}O$. The interaction of the magnetic dipole moment with the geomagnetic field leads to a Zeeman splitting of the O_2 rotational transitions. This effect was studied by Gautier[1] and Lenoir[2,3] in the 60 GHz band of the main isotope $^{16}O_2$. Liebe[4] modeled it with a realistic geomagnetic field. It appears, from these works, that the Earth's magnetic field splits the different Zeeman components over a range of a few MHz around the centre of each rotational line. The shape of each component is governed by a pressure broadening mechanism up to $\sim$60 km of altitude, and by a Doppler mechanism above. The $^{16}O_2$ rotational lines appear optically thick for ground observations. This fact prevents observation of any Zeeman substructure which can be seen only from satellite by means of limb soundings. Some measurements have been carried out for the $9_9 \rightarrow 9_{10}$ (N_J notation) line of $^{16}O_2$ at 61.15056 GHz (Hartmann et al[5]) that are compatible with model calculations. But the frequency resolution of the M.A.S. instrument, used for these measurements, is too poor to clearly see the substructure. However, for temperature soundings of the atmosphere at high altitudes using satellite measurements close to $^{16}O_2$ rotational resonances, this effect cannot be neglected.

For the much rarer isotopic species $^{16}O^{18}O$, that has a relative abundance of $(^{16}O^{18}O/^{16}O_2) = 2^{8}O/^{16}O = 4.09 \cdot 10^{-3}$ in the atmosphere, the emission from upper atmospheric layers can be

§To whom all correspondence should be addressed.

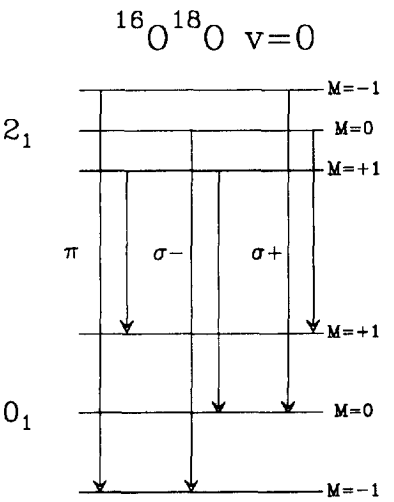

Fig. 1. Scheme of the Zeeman sublines within the rotational transition $2_1 \rightarrow 0_1$ of the $^{16}O^{18}O$ molecule. Six components are expected following the selection rules.

observed and the Zeeman substructure appears detectable from the ground. We have chosen the $2_1 \rightarrow 0_1$ line of $^{16}O^{18}O$ at 233,946.11 MHz to try to detect this effect and to study its direction and polarization dependence.

Starting from the ZPM model of Liebe,[4,6] that simulates the anisotropic propagation of a radio wave in the Earth's atmosphere at a frequency close to a $^{16}O_2$ resonance around 60 GHz, we have extended it to the submillimetric $^{16}O_2$ lines (368.498, 424.763, 487.249 GHz, etc.) and the $^{16}O^{18}O$ lines at 233.946 GHz and higher frequencies. We have also introduced some modifications in order to calculate brightness temperature matrices in different polarization bases as defined by Lenoir.[2]

Six Zeeman components are expected for the observed $^{16}O^{18}O$ line if we take into account the selection rules: $\Delta M = 0, \pm 1$ ($0 \rightarrow 0$ is forbidden) (see Fig. 1). Lines with $\Delta M = \pm 1$ are called $\sigma \pm$ components, and those with $\Delta M = 0$ are known as π components. It is well known that the π patterns arise from interactions with the gas of a radio-wave that is linearly polarized in the direction of the geomagnetic field vector, and the $\sigma \pm$ components are excited by magnetic wave vectors that are right-hand and left-hand circularly polarized in the plane perpendicular to $\boldsymbol{B}$. So, depending on the line of sight and the orientation of the polarization of the receiver, the profile of the line must be different.

We will present in Sec. 2 a description of the instrument and the observations. Sections 3 and 4 will be a brief review of the theory involved in the model. In Sec. 5 we discuss and interpret the results of our observations and their agreement with the model predictions. Finally, in Sec. 6 we give our conclusions and a discussion of future T-soundings near $^{16}O_2$ resonances that need to take into account the Zeeman effect.

2. OBSERVATIONS

The observations were made from the 14th to the 19th of January 1995 at the POM-2 telescope (Castets et al[7]). The POM-2 focal instrument has been much improved since its original installation mainly by replacing the Schottky diode mixer with an SIS mixer of temperature Trec (DSB) $= 65 \pm 10$ K. However, at the time of these observations, a temporary problem degraded the receiver up to 120 K. The forward efficiency (η_f which represents the coupling of the telescope with the sky) reaches 0.82. Depending on the weather, the system temperature ran from 600 to 800 K which takes into account the sky opacity (from 0.13 to 0.25 neper towards the zenith, mostly due to water vapour absorption). This means that the data were automatically corrected as if they were coming from outside the atmosphere (astrophysical lines) which is not true here (but acceptable for CO atmospheric emission observations, for example, which take place at very high altitude, much above the bulk of the absorbing layers). Offline, this sky opacity correction was removed to yield the intensity at the ground level for the corresponding elevation. The water vapour content towards

zenith was estimated to be between 1.3 and 2.8 mm of precipitable water from day to day. The observations were done in differential mode, by subtracting a reference spectrum to the signal. This was done by changing the receiver frequency to displace the line centre inside or even outside the backend range. The receiver backend was set to work at different resolutions: 39, 78 and 156 kHz with total bandwidth in the range 4.53–36.25 MHz depending on the frequency throw of the frequency switching mode. Because the line is broader than the frequency throws, the zero level in the spectrum cannot be traced with high accuracy because the influence of the line wings is not well known. Nevertheless, this problem is not critical here because we are interested to compare only the simulated and observed profiles. Quantitative agreement would need the use of the true atmosphere in the calculations and a broad backend in the observations in order to correctly estimate the continuum level. For the low resolution case, the throw was 40 MHz for the reference spectrum, displacing the line centre outside the backend while for the high resolution mode, the throw was ± 2.265 MHz, to keep the line centre always inside the backend. This has the advantage to improve the signal-to-noise ratio faster because the line is always observed. The r.m.s. deviation runs from 70 mK for the high resolution spectra to 150 mK for the low resolution spectra.

3. GENERALIZED RADIATIVE TRANSFER EQUATION

In order to interpret these observations, it is necessary to study the propagation of partially polarized electromagnetic waves in a slightly anisotropic medium. Therefore we need a generalized form of the radiative transfer equation.

From Maxwell's equations, the propagation of a plane wave travelling in the $+z$ direction is described, in terms of its associated magnetic field by

$$\frac{\partial^2}{\partial z^2} H(z, \nu) - G^2(\nu) H(z, \nu) = 0 \tag{1}$$

for which the solution is

$$H(z, \nu) = \exp[-G(\nu)z] H(0, \nu) \tag{2}$$

where $G(\nu)$ is a propagation matrix in the polarization plane. This matrix depends on the physical properties of the medium. In this case, the medium has a scalar permittivity ϵ_0 and a tensor of magnetic permeability $\mu = \mu_0[I + \chi(\nu)]$ [with $\chi_{ij}(\nu) \to 0$, for the case of weak magnetic field]. The relation between $G(\nu)$ and these physical properties is

$$G(\nu) = ik_0[I + \tfrac{1}{2}\chi(\nu)] \tag{3}$$

$$k_0^2 = 4\pi^2 \nu^2 \epsilon_0 \mu_0 \tag{4}$$

From Maxwell's equations, it is also possible to know the associated electric field. For that, it is suitable to use a false vector $E_p(z, \nu)$ ($E_{px} = -E_y$, $E_{py} = E_x$)

$$E_p(z, \nu) = \frac{G(\nu)}{i2\pi\nu\epsilon_0} H(z, \nu) \tag{5}$$

We are interested in the energy flow that arrives to our detector due to natural emission and propagation through the atmosphere. So, we need to calculate the time average ($\langle \ldots \rangle$) of the Poynting's vector. For this purpose Lenoir[2] used a complex power-spectrum coherency matrix (Born and Wolf[8])

$$S_{ij}(\nu) = \langle E_{pi}(\nu) H_j^*(\nu) \rangle \tag{6}$$

that can be decomposed into its hermitian ($P = P^{*T}$, $*$ and ^{T} being the conjugated and transposed operations respectively) and anti-hermitian parts

$$S(\nu) = P(\nu) + iQ(\nu) \tag{7}$$

The hermitian part $P(\nu)$ is interesting for us because its trace is equal to the time average power flowing in the $+z$ direction. The main diagonal elements P_{xx} and P_{yy} are real and non-negative. They represent, respectively, the power spectra for x-linear and y-linear polarizations, if the vectors

representing these two states are the base that has been chosen to describe the polarization of the wave. Off-diagonal elements are a measure of the coherence between these polarizations.

In the scalar case, at millimeter wavelengths, we have a linear relationship between power and brightness temperature given by the Rayleigh-Jeans approximation ($kT \gg hv$)

$$dP_0(\theta, \phi) = \frac{kT_B(\theta, \phi)}{\lambda^2} d\Omega \tag{8}$$

Following the same way, Lenoir[2] defines a brightness temperature matrix $T_B(v)$ that obeys all the conditions and mathematical rules of $P(v)$.

Finally, we must find an equation describing how the matrix $T_B(z, v)$ changes when the wave propagates in the $+z$ direction. Such an equation will be equivalent to that of $P(z, v)$ due to the relationship between these two matrices.

From Maxwell's equations and the above definitions we have (1st order)

$$\frac{\partial}{\partial z} E_p(z, v) = -i2\pi v\mu_0[I + \chi(v)]H(z, v) \tag{9}$$

$$\frac{\partial}{\partial z} H(z, v) = -i2\pi v\epsilon_0 E_p(z, v) \tag{10}$$

If we multiply (9) by $H^{*T}(z, v)$ and add it to the conjugated transposed of (10) premultiplied by $E_p(z, v)$, we get

$$\frac{\partial}{\partial z} E_p H^{*T} = -i2\pi v\mu_0[I + \chi(v)]HH^{*T} + i2\pi v\epsilon_0 E_p E_p^{*T} \tag{11}$$

using the relation between E_p and H [Eq. (5)], that leads to

$$\frac{\partial}{\partial z} E_p H^{*T} + G(v)E_p H^{*T} + E_p H^{*T} G^{*T}(v) = 0 \tag{12}$$

Finally, if we take the time average of (12), we get a differential equation for the coherency matrix $S(v, z)$ that is

$$\frac{\partial}{\partial z} S(z, v) + G(v)S(z, v) + S(z, v)G^{*T}(v) = 0 \tag{13}$$

This equation can be separated in two parts, one for the hermitian part of $S(z, v)$ and another one for the antihermitian part. The equation for the hermitian part $P(z, v)$ can be expressed also in terms of $T_B(z, v)$ if we take into account relation (8)

$$\frac{\partial}{\partial z} T_B(z, v) + G(v)T_B + T_B G^{*T}(v) = 0 \tag{14}$$

This equation does not include the emission from the medium. In order to do that, we must take into account that the change in T_B per unit length plus the loss of T_B per unit length equals the emission per unit length

$$\frac{\partial}{\partial z} T_B(z, v) + G(v)T_B + T_B G^{*T}(v) = E(v) \tag{15}$$

An important simplification occurs when the medium obeys the thermodynamic equilibrium. Then $(\partial/\partial z)T_B(z, v) = 0$ and we obtain the next relation between absorption and emission

$$G(v)T_e + T_e G^{*T}(v) = E(v) \tag{16}$$

where T_e is known as the emission temperature matrix (for thermal emission) of the medium. General radiative transfer equation is obtained substituting (16) into equation (15)

$$\frac{\partial}{\partial z} T_B(z, v) + G(v)T_B + T_B G^{*T}(v) = G(v)T_e + T_e G^{*T}(v) \tag{17}$$

The general solution of this equation, for a homogeneous layer in which the incident brightness temperature matrix is $T_B(0, \nu)$ and the emission temperature matrix is $T_E(\nu)$, is

$$T_B(z, \nu) = e^{-G(\nu)z} T_B(0, \nu)\, e^{-G^* T(\nu)z}(0, \nu) + T_e(\nu) - e^{G(\nu)z} T_e(\nu)\, e^{-G^* T(\nu)z} \tag{18}$$

In our case (Earth's atmosphere), the emission temperature matrix will be diagonal with its nonzero elements equal to the kinetic temperature of the layer $[T(z)]$. Then, in the third addend of the right hand of equation (18) $T_e(\nu)$ commutes with the exponential of $G(\nu)$, and only its hermitian part $[A(\nu)]$ remains. So, the final expression for the solution of the generalized radiative transfer equation is

$$T_B(z, \nu) = e^{-G(\nu)z} T_B(0, \nu)\, e^{-G^* T(\nu)z} + T[I - e^{-2A(\nu)z}] \tag{19}$$

4. ZEEMAN SPLITTING OF MILLIMETRIC AND SUBMILLIMETRIC O_2 LINES IN THE EARTH'S ATMOSPHERE

The Earth's magnetic field has a variable intensity within the range of ~ 22–$65\ \mu T$ that spreads the Zeeman components of the O_2 rotational spectrum over a frequency range of a few MHz typically. In the upper stratosphere and in the mesosphere this effect becomes important due to the fact that the O_2 lines appear very narrow due to the low pressures, and the width becomes of the same order as the Zeeman splitting. While, as we said in the introduction, the upper stratospheric and mesospheric emission of the main isotope $^{16}O_2$ cannot reach detectors at ground level, this is not true for $^{16}O^{18}O$ lines of much lower opacity.

Using the theory exposed in Sec. 3 we now review how to model the brightness temperature in the vicinity of the millimetric and submillimetric O_2 resonances. As it was pointed out by Rosenkranz and Stealin,[10] the hermitian and antihermitian part of $G(s, \nu)$ do not commute in general. However, when the angle between the magnetic field and the direction of propagation is 0°, 90°, or 180°, A and B commute and then we can write the generalized radiative transfer equation as

$$T_B(z_f, \nu) = e^{-A_i \Delta z} T_B(z_i, \nu)\, e^{-A_i^* T \Delta z} + T[I - e^{-2A_i \Delta z}] \tag{20}$$

to calculate the brightness temperature matrix at the end of a layer as a function of its initial value. For other angles, the antihermitian part $B(s, \nu)$ remains in the last equation. This fact introduces mainly a Faraday rotation in the polarization ellipse. For our chosen observation directions the last equation may be used. The influence of the antihermitian part of G on the diagonal elements of T_B for different angles between $\boldsymbol{B}$ and the direction of propagation was investigated also by Rosenkranz and Stealin[10] for a $^{16}O_2$ line centered at 60.43478 GHz. Their results show negligible differences for practical observations.

In order to show which layers have a non-negligible contribution to the T_B measured from the ground or from satellite, Eq. (20) is written in terms of the so-called monochromatic temperature weighting function matrix $[W(i, \nu)]$

$$T_B(w) = \sum_{i=1}^{n_{\text{layers}}} W(i, \nu) T\left(z_i + \frac{\Delta z_i}{2}\right) \tag{21}$$

(a contribution of the Earth's surface for satellite observations or of the cosmic background for ground-based measurements must be added for some cases where the total atmospheric transmission is not zero).

Figure 2 shows some calculations of the diagonal elements of this matrix for one of the cases that will be presented here, in order to show that the ground-based observations of the $2_1 \rightarrow 0_1$ $v = 0$ $^{16}O^{18}O$ line are sensitive up to ~ 65–70 km. Pressures of the order of 0.2 mb are expected at altitudes of around 58–60 for a standard atmospheric model, which should give Zeeman subline halfwidths of the order of 1 MHz that corresponds approximately with the substructure we can see on the next figures.

Now we must calculate the attenuation matrix A. For the $^{16}O_2$ molecule, many works (Gautier,[1] Lenoir,[3] Liebe[6]) have been developed on the Zeeman effect over the spin-rotation spectrum due to transitions with unchanged rotational momentum (N) and total angular momentum (J) that changes from N to $N+1$ ($N+$ lines) or to $N-1$ ($N-$ lines) [both ($N, J = N-1$) and

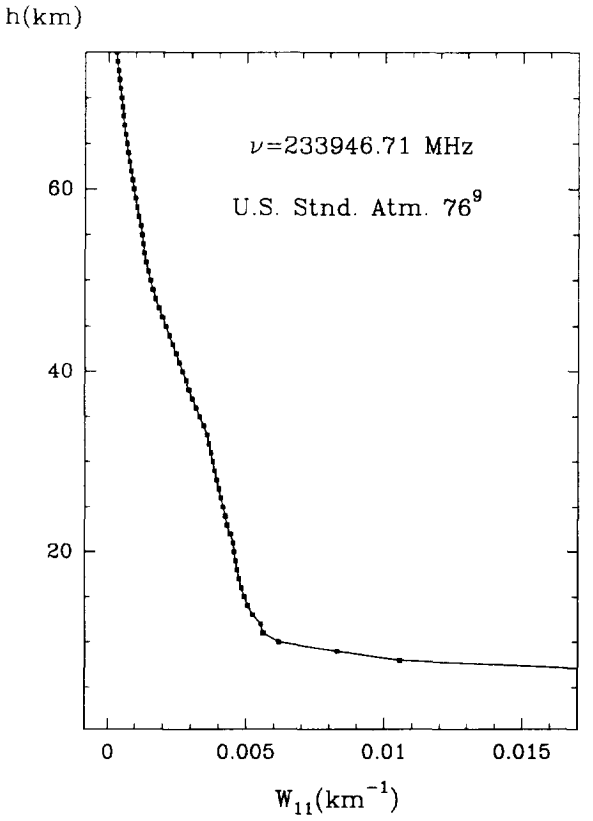

Fig. 2. Diagonal elements of the weighting matrix $W(i, v)$ using the U.S. Standard Atmosphere 1976[9] at a frequency offset of 0.6 MHz from the centre of the line presented in this paper. The line-of-sight is parallel to the Earth's magnetic field. We see that the contribution to the measured T_B is non negligible up to 70 km.

$(N, J = N + 1)$ energy levels are lower than $(N, J = N)$]. These studies include the 60 GHz $^{16}O_2$ band and an isolated line at 118.75 GHz (1_-), but do not include other interesting lines in the submillimetric range (starting at 368.498 GHz) that are transitions where $\Delta N = -2$ (for emission). Each energy level (N, J) splits due to the Zeeman effect into $2J + 1$ levels described by the quantum magnetic number M. Selection rules for M are $\Delta M = 0, \pm 1$. Emission of these lines is polarized and must be described by means of coherency matrices. Lenoir[3] who uses the magnetic field of the wave in order to describe its propagation [eq. (2)] gives these coherency matrices in a base of the plane of polarization where the two vectors represent linear polarization along N–S and E–W magnetic directions. The model ZPM of Liebe[6] carries out the propagation of the wave in terms of its electric field

$$E_z = \exp[ikz(I + N_z 10^{-6})]E_0 \tag{22}$$

where N_z (in ppm) is a 2×2 refractivity matrix in the plane of polarization defined by Liebe from the work of Lenoir.

In general, when the propagation is contained in a $S_{mag} - N_{mag}$ plane the V-polarization in the sky follows the N–S magnetic direction and the H-polarization has the orientation E–W. In this case, we can write the refractivity matrix for the VP–HP base like this

$$\begin{bmatrix} N_0 \sin^2\phi + (N_+ + N_-)\cos^2\phi & -i(N_- - N_-)\cos\phi \\ i(N_+ - N_-)\cos\phi & N_+ + N_- \end{bmatrix}$$

where ϕ is the angle between the magnetic field and the direction of propagation. N_0 and $N_\pm$ are the Zeeman refractivity patterns for the π and $\sigma_\pm$ transitions. These patterns are calculated as the total line intensity, times a normalized relative line strength for each Zeeman component, times a normalized line shape factor. This line shape factor is a single Lorentzian profile with a correction for the halfwidth parameter in order to take into account the Doppler-broadening, that becomes

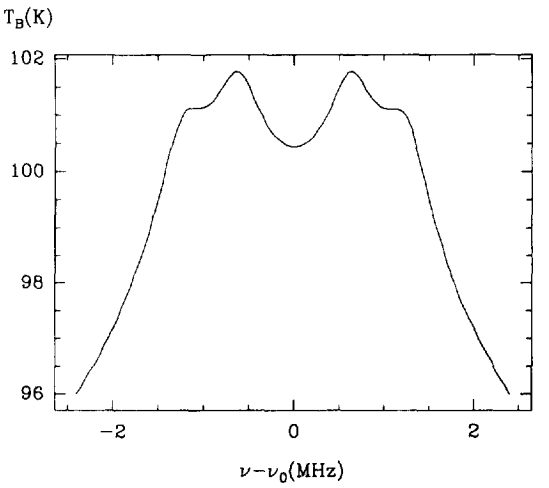

Fig. 3. Model predictions for the profile of the $2_1 \rightarrow 0_1$ $^{16}O^{18}O$ line for a line-of-sight almost parallel to the geomagnetic field around Plateau de Bure. Only two of the six components appear clearly. The atmospheric profile used for the calculations was U.S. Standard Atmosphere 1976.[9]

non negligible for altitudes above ~ 60 km. In order to get the right matrix in the case $\boldsymbol{B} = 0$, the relative line strengths χ_M must verify $\Sigma\chi_M = 1$ for N_0 and $\Sigma\chi_M = 0.5$ for $N_\pm$. Lenoir and Liebe in their works give the relative line strengths for the Zeeman substructures only for lines $\Delta N = 0$ and $\Delta J = \pm 1$ as we said above. However, the submillimetric $^{16}O_2$ lines and the $^{16}O^{18}O$ lines are cases where both quantum numbers N and J change. So, we must apply the rigorous expressions for the line strength that can be found in the original work of Tinkham and Strandberg.[11,12]

The total line intensity is usually calculated from the line strength parameter (λ_g), which is defined from the matrix element of the dipole moment of the transition (μ)

$$|\langle J, \tau | \mu | J', \tau' \rangle|^2 = \frac{\mu_g^2 \lambda_g(J, \tau, J', \tau')}{(2J+1)} \tag{23}$$

where g represents the spatial direction of the dipole moment, J is the total angular momentum, and τ, τ' are other quantum numbers. For the line we study $\lambda_g = 0.776$.

For the pressure-broadening parameters of the $2_1 \rightarrow 0_1$ $^{16}O^{18}O$ line we adopt the law $\gamma = aPT^x$ with $a = 6.01$ MHz/mb and $x = 0.2$ as given by Liebe[6] for the submillimetric lines of the main isotope $^{16}O_2$ at 368.5, 424.8, and 487.2 GHz.

It is necessary to add, of course, the continuum and the wings of other lines, that is a scalar contribution included in the diagonal elements of the refractivity matrix (Liebe[13]).

Mutual incoherence of the Zeeman components is assumed in order to calculate N_0 and $N_\pm$. So, the matrix N_z is hermitian and, in addition, $\mathrm{Re}(N_{z,ij}) = 0$, $i \neq j$. That means, if we look at Eq. (20), that the T_B matrix has also $\mathrm{Im}(T_{Bii}) = 0$ and $\mathrm{Re}(T_{Bij}) = 0$, $i \neq j$. In general, as we explained, this fact is a consequence of neglecting the phase terms represented by the antihermitian part of G, and it is exact for propagations following the parallel or perpendicular directions to the magnetic field. So, there is never a linear coherence between T_{B11} and T_{B22}, meanwhile σ components have circular coherence given by the off-diagonal T_B elements.

5. PREDICTIONS AND RESULTS

The central frequencies of each Zeeman component are calculated from the splitting of the energy levels, given by

$$\Delta E = -1.00010\mu_0 MH \cdot \frac{J(J+1) + S(S+1) - N(N+1)}{J(J+1)} \tag{24}$$

where $S = 1$ for O_2, μ_0 is the Bohr magneton, H is the strength of the external magnetic field, and ΔE is the energy change from the centre of the N_J level. The quantum factor is equal to -1 for

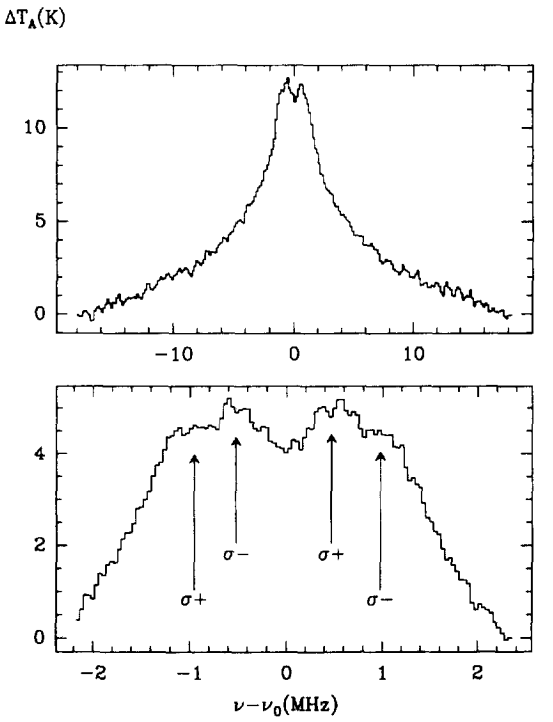

Fig. 4. Two observations carried out with the millimetric radiotelescope POM-2 for AZM = −2° and ELV = 59° using different bandwidths. The flat regions in both wings of the spectrum are identified as two other σ components.

the upper level (2_1), and to 2 for the lower one (0_1). It means that the frequencies of the transitions can be calculated from the next equation

$$\Delta\nu(GHz) = 14.015 \cdot 10^{-6} H_{\mu T}(M_u + 2M_l) \tag{25}$$

We can see in Fig. 1 the energy level diagram and the line identification. We know that the range of the geomagnetic field strength is 22–65 μT, so, the Zeeman substructure will appear in a region of a few MHz around the central frequency. For this reason we must use the highest frequency resolutions available in the backends of the present millimetric radiotelescopes (40–20 kHz) in order to clearly see the structure we are searching.

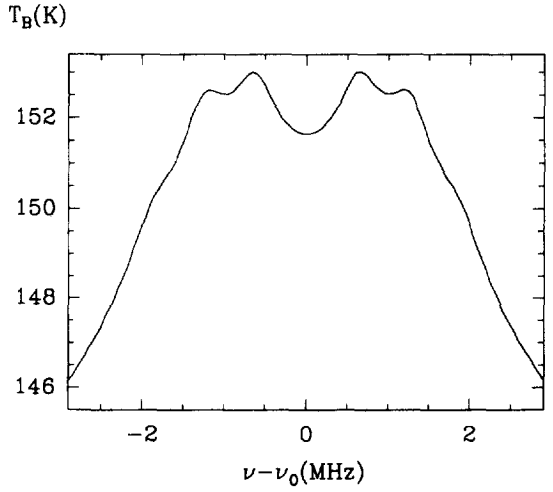

Fig. 5. Model predictions when the telescope is pointed almost perpendicular to the geomagnetic field around Plateau de Bure. We clearly see the four σ components. A slight distortion in the line wings is associated to the two π components.

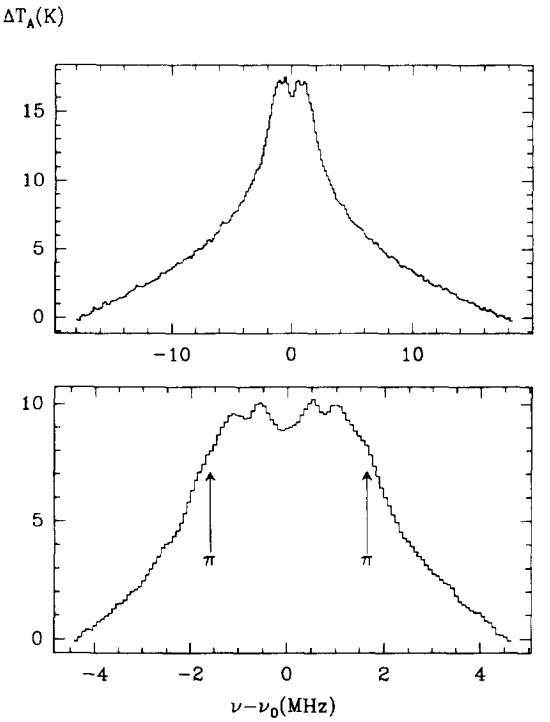

Fig. 6. The observations for the case presented in the last figure agree very well with the model. Only the π components remain undetected.

From the discussions of the last section, it is obvious that the model calculations are simplified if we consider a radio-wave that propagates in a plane that contains the two magnetic poles. It means that the telescope must point in a direction with azimuth $N_{mag} - S_{mag}$ or close to it.

If we choose a line of sight parallel to the magnetic field, the refractivity matrix for the (VP, HP) base equals to

$$\begin{bmatrix} N_+ + N_- & -i(N_+ - N_-) \\ i(N_+ - N_-) & N_+ + N_- \end{bmatrix}$$

Then, we can only detect the 4 peaks associated to the $\sigma_\pm$ patterns. Figure 3 shows the model predictions for a line of sight at -2° of azimuth (0° = South) and elevation = 59° for Plateau de

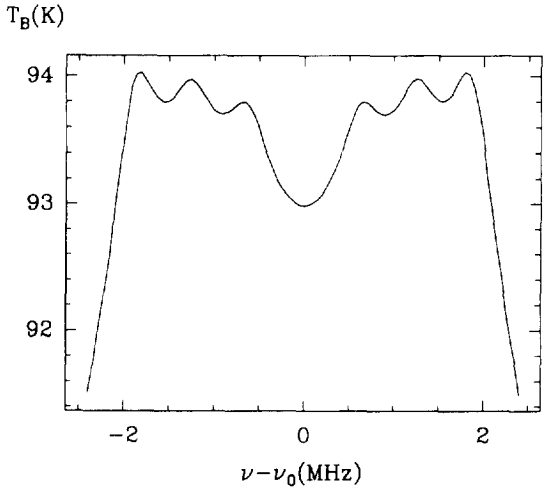

Fig. 7. If we take into account the polarization of the receiver of the POM-2 radiotelescope, the direction AZM = 178°, ELV = 70° appears suitable to detect the π components of the $^{16}O^{18}O$ line, as we can see in these model calculations.

Bure, that corresponds to a direction almost parallel to the geomagnetic field. There are two inner peaks clearly seen and two flat external structures that are associated to the other two σ components. We have taken two spectra with different bandwidths and frequency resolutions that are shown in Fig. 4. The first one (largest band) shows the existence of two peaks (evidence of the Zeeman substructure), but there is not enough resolution to see the flat structure associated to the two external σ sublines. The second one shows a very good agreement with the predicted profile.

In order to detect the π components, we have to point the telescope in the direction perpendicular to the geomagnetic field (AZM = 178°, ELV = 27°). From the expression of N_z it appears that, in this case, the π components have a vertical polarization in the sky. The radiation reaches the receiver of POM-2, which is sensitive to a linear polarization parallel to the ground (horizontal), after a reflection on a mirror rigidly rotating with the parabola. For this reason, the polarization seen by the receiver in the sky changes from H (for ELV = 0°) to V in the limit ELV = 90°. So, we must apply a rotation matrix of 27° to the refractivity matrix in the calculations in order to get the expected profile for this case (we did also a rotation of 59° for the calculations presented in Fig. 3, but the effect in that case can be neglected because the refractivity matrix in the LV–HV base has equal diagonal elements with its off-diagonal elements very small). Since 27° is a low elevation, the receiver sees mainly the H-polarization in the sky and the π components do not appear clearly. There are, however, some slight distortions in the line wings associated to the π components. In that direction the four σ peaks appear clearly in the model (Fig. 5) that is successfully confirmed by the observations (Fig. 6).

In order to clearly detect the π components, we pointed to the same azimuth but at higher elevation (70°). In this case, the π components are weaker due to the fact that the line of sight is not perpendicular to the magnetic field. However, the receiver becomes mostly sensitive to the V-polarization in the sky, making possible the unequivocal identification of the π components. The simulations show the six sublines, but the contrast is low (Fig. 7). Then, with the same time of integration than the other observations it will be difficult to distinguish the peaks above the noise level. However, the line may appear broader due to the contribution of the external π components. In fact, if we superimpose the observations at 27° and 70° of elevation, correcting for the effect of the different air masses, we clearly see a large difference due to the π components (Fig. 9).

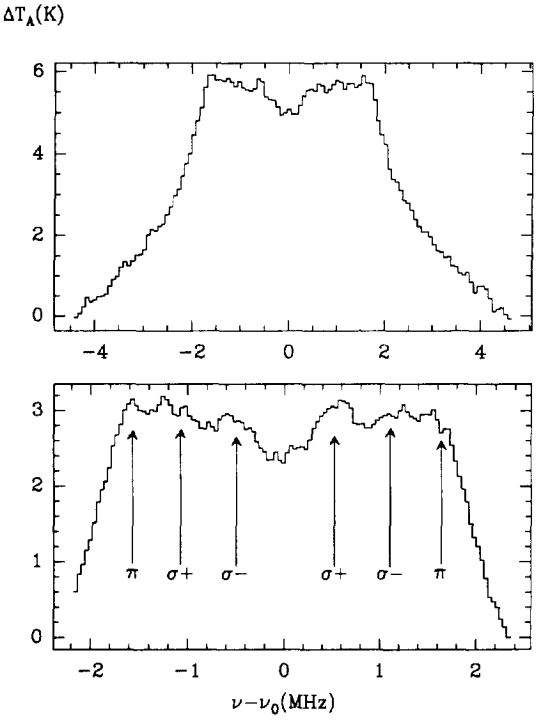

Fig. 8. These observations show evidence for the π components of the Zeeman substructure of the 233.94611 GHz $^{16}O^{18}O$ line.

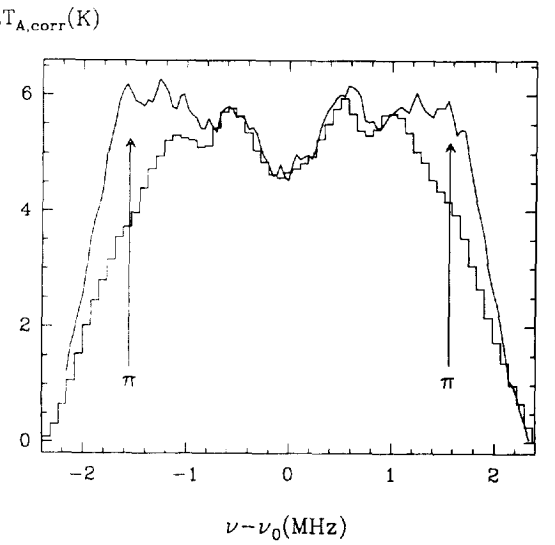

Fig. 9. The comparison, after correction of the effect of the air mass, between the observations at the same azimuth and ELV = 27° and 70° proves that the π components are associated to the V-pol in the sky at this azimuth, because they must be weaker at 70° but appear stronger due to the higher sensitivity of the system to the V-pol in the sky at this elevation.

Obviously, for the three cases presented here the angle between the direction of propagation and the geomagnetic field for the atmospheric region where the detected radiation originates (in the model we take 0–130 km because ionospheric effects follow a ν^{-2} law and could be neglected for $\nu > 3$ GHz) is not constant. However, the variations are small: for the chosen "perpendicular" line of sight $z \perp \boldsymbol{B}$, this angle changes from 87.8° at 130 km to 91.6° at 2.5 km according to Barraclough et al.[14] For the "parallel" case this angle has values between 1.3° and −0.1°, and 48.9° to 49.5° for the observation at ELV = 70°. The figures show that a systematic offset remains in all cases when we compare the expected positions of the peaks and the observed one. For the good spectra taken in the "perpendicular" case with a resolution of 84 kHz we have calculated that the averaged value of the magnetic flux density over Plateau de Bure would be of $\sim 40\,\mu$T that represents a difference around 10% with the standard model ($\sim 44\,\mu$T). This difference may be too large compared to the possible deviations to the standard magnetic model used. Potential sources of deviations are: ionospheric effects, changes in the Earth's magnetic field (around 50 nT/year) from 1980 (year of the measurements on which is based the model of Barraclough et al[14]), and local deviations of this model that describes $\boldsymbol{B}_{geo}$ over scales of ~ 1000 km. However, if we take into account the errors of our determination of $\boldsymbol{B}$, due to the noise level and frequency resolution of our spectra, agreement is possible.

Bergman[15] obtained a spectrum of the same $^{16}O^{18}O$ atmospheric line with the SEST radiotelescope located at La Silla (Lat. 29:15:24 S, Long. 70:43:48 W, Alt. 2347 m) in Chile with a lower frequency resolution. The receiver of this telescope moves together with the whole antenna. The polarization detected in the sky is always LV. So, from our model calculations, the observation to the direction perpendicular to the geomagnetic field must show clearly the π peaks. This point has been confirmed by the observation. σ peaks were not detected. The frequency resolution and observational noise prevents from setting the central position of the peaks with high accuracy. We can say, however, that the spectrum is consistent with a mean value of $\boldsymbol{B}_{Geo}$ over La Silla of 25 μT with estimated error of 10% which is in agreement with the value given by the geomagnetic field model of Barraclough et al.[14]

6. SUMMARY AND CONCLUSIONS. RELATED WORKS

We have extended previous models of the geomagnetic Zeeman effect on $^{16}O_2$ rotational lines to the submillimetric ($\Delta N = -2$) transitions of this molecule and the main lines of its isotopic species $^{16}O^{18}O$. This theoretical work has allowed us to predict the profile of the $2_1 \rightarrow 0_1$ $^{16}O^{18}O$ line

for ground observations in different orientations. Pointing the millimetric telescope POM-2 to three chosen directions we have clearly detected the six Zeeman sublines that are expected from the selection rules. In order to correctly interpret the results we have taken into account the polarization sensitivity of the receiver and its projection in the sky after reflection on a mirror.

This work is an effective test of the model that must be used for calculations in order to do the inversion of the data of different future upper stratospheric and mesospheric T-sounders on board satellites, that will have some channels at frequencies very close to the $^{16}O_2$ resonances around 60 GHz (SSMIS, AMSU-A, . . .) where the geomagnetic Zeeman effect must be taken into account.

In order to carry out these kinds of studies there are some projects that have proposed different choices for the frequencies (always in the 60 GHz band of $^{16}O_2$) and polarization of the channels (linear or circular). These systems fix the local oscillator frequency of the upper atmospheric channels between two strong $^{16}O_2$ peaks and the upper and lower side bands are placed at the same absolute frequency offset from the two peaks. In order to cover an altitude range from 40 to 70 km these channels must be separated from the line center by 5 and 0 MHz. The temperature weighting matrix shows in general a double peak in the *HL–VL* base for $\nu - \nu_c$ of the order of 1 MHz because each polarization (*HL* and *VL*) mixes the two circular polarizations that have the peaks associated to their weighting functions at different altitudes. To avoid this problem, Rosenkranz and Stealin[10] suggest to work in circular polarization with the couple of lines 7+ and 9+ (additional channels for AMSU-A, see Table 1). However, a technical problem appears from this choice: the polarization of the two sidebands needs to be reversed because the lines appear asymmetric in *LC* or *RC* polarization, the upper wing of the 7+ line in *RC* being equivalent to the lower wing of the 9+ in *LC*.

In order to avoid this problem Bommarito et al[16] give a channel choice for the instrument SSMIS that essentially conserves the frequencies around the 7+ and 9+ lines (except for $\nu - \nu_c \simeq 1$ MHz) working in linear polarization. In order to cover a "hole" around 60 km in the altitude coverage of the weighting functions, they propose a channel centered on the weaker peaks 15+ and 17+. The altitude coverage is similar but the technical inconvenient is now the necessity of two local oscillator frequencies.

In the Department of Millimeter Radioastronomy (DEMIRM) of the Observatoire de Paris we have carried out a study for the choice of channels of a T-sounder based on a "push-broom" concept (see Tabart[17]) for the CNES (Centre National d'Etudes Spatiales, France). For lower atmosphere channels we use the same definition of AMSU-A. For upper atmosphere we consider technically preferable to work in linear polarization. But we choose our frequencies below 60 GHz for multiple reasons: the total set of channels (taking into account lower atmosphere channels) is

Table 1. Different choices for upper atmosphere channels of some future T-sounders. The inversion of the data from these channels needs to take into account the geomagnetic Zeeman effect.

ν_c(GHz)	$\Delta\nu$(MHz)	Sensib. δT(K)	Polariz.
AMSU-A (NOAA) upper atmosphere channels			
60.79267 ± 0.3539	±1.5	1.5	*LC* + *RC*
60.79267 ± 0.3558	±0.4	2.8	*LC* + *RC*
60.79267 ± 0.3569	±0.25	3.5	*LC* + *RC*
60.79267 ± 0.3579	±0.5	2.5	*LC* + *RC*
60.79267 ± 0.3589	±0.25	3.5	*LC* + *RC*
60.79267 ± 0.3600	±0.4	2.8	*LC* + *RC*
SSMIS (DMSP) upper atmosphere channels			
63.2832 ± 0.2853	—	1.9	*H* + *V*
60.7927 ± 0.3579	—	1.9	*H* + *V*
60.7927 ± 0.3581	—	1.4	*H* + *V*
60.7927 ± 0.35845	—	1.0	*H* + *V*
"Push-Broom" (CNES) upper atmosphere channels			
56.665797 ± 0.30241	±0.4	—	*H* + *V*
58.744042 ± 0.42020	±0.4	—	*H* + *V*
58.744042 ± 0.41820	±0.4	—	*H* + *V*
58.744042 ± 0.41720	±0.4	—	*H* + *V*
58.744042 ± 0.41570	±0.4	—	*H* + *V*

more compact, the water vapor continuum is less important at lower frequencies and, finally, the actual situation of frequency sharing between passive and active services gives an exclusive use for active services between 59.0 and 64.0 GHz while the allocation is exclusive for passive services between 58.2 and 59.0 GHz and shared from 54.25 to 58.2 GHz. Table 1 shows these channel choices.

Other systems on board satellites will be able to carry out limb soundings for sub-millimetric $^{16}O_2$ lines. For example, the future ODIN satellite (Sweden, France, Canada) will be equipped with spectrometers of 1 MHz and 100 kHz of frequency resolution that could show evidence of the Zeeman splitting in the $3_3 \rightarrow 1_2$ line of $^{16}O_2$ (487.25 GHz) and apply it to mesospheric temperature studies.

Acknowledgements—J. R. Pardo gratefully acknowledges the financial support of the Observatoire de Paris–Meudon and the use of its facilities during the development of this work. We thank also the Observatoire de Grenoble for allowing us the use of the POM-2 radiotelescope and for its financial support during the observations at Plateau de Bure. J. R. Pardo and C. Prigent acknowledge Professor H. J. Liebe for providing us with his ZPM model that has been the starting point of this work. We also thank the Spanish CICYT that has partially supported this work, under project PB90-408.

REFERENCES

1. D. Gautier, Ph.D, Univ. de Besançon, GRI/NTP/12 (1969).
2. W. B. Lenoir, *J. appl. Phys.* **38,** 5283 (1967).
3. W. B. Lenoir, *J. geophys. Res.* **73,** 361 (1968).
4. H. J. Liebe, *Radio Sci.* **16,** 1183 (1981).
5. G. K. Hartmann et al, Zeeman splitting of the 61 GHz (9+) O_2 line in the mesosphere, personal communication (Oct. 1993).
6. H. J. Liebe et al, *AGARD 52nd meeting*, Mallorca, Spain (1993).
7. A. Castets, R. Lucas, B. Lazareff et al, *Astron. Astrophys. 194*, 340 (1988).
8. M. Born and E. Wolf, *Principles of Optics*, 2nd edition, Pergamon Press, Oxford (1964).
9. "U.S. Committee on Extension to the Stnd. Atm.", U.S. Printing Office, Washington D.C. (1976).
10. P. W. Rosenkranz and D. H. Stealin, *Radio Sci.* **23,** 721 (1988).
11. M. Tinkham and M. W. Strandberg, Theory of the fine structure of the molecular oxygen ground state, *Phys. Rev.* **97,** 937 (1955).
12. M. Tinkham and M. W. Strandberg, Interaction of molecular oxygen with a magnetic field, *Phys. Rev.* **97,** 951 (1955).
13. H. J. Liebe, *Int. J. Infrared Millimeter Waves* **10,** 631 (1989).
14. D. R. Barraclough, International Geomagnetic Reference Field revision 1985, *Pure Appl. Geophys.* **123,** 641 (1985).
15. P. Bergman, School of Electrical and Computer Engineering, Chalmers Univ. of Tech., Sweden, Tech. Report No. 227 (1992).
16. J. Bommarito, *Microwave Instrumentation for Remote Sensing of the Earth* (ed. C. Shine), ISPIE Meeting, Orlando, Florida (Apr. 1993).
17. C. Tabart, Ph.D., Univ. Pierre et Marie Curie, Paris (1991).